Bulk and surface transitions in asymmetric simple exclusion process: Impact on boundary layers

Sutapa Mukherji and Vivek Mishra
Department of Physics, Indian Institute of Technology, Kanpur 208016, India
(Received 10 January 2006; published 24 July 2006)

In this paper, we study the boundary-induced phase transitions in a particle nonconserving asymmetric simple exclusion process with open boundaries. Using a boundary layer analysis on the mean field version of the model, we show that the key signatures of various bulk phase transitions are present in the boundary layers of the density profiles. In addition, we also find surface transitions in the low- and high-density phases. The surface transition in the low-density phase provides a complete description of the nonequilibrium critical point found in this system.

DOI: 10.1103/PhysRevE.74.011116 PACS number(s): 64.60.−i, 05.40.−a, 02.50.Ey, 89.75.−k

I. INTRODUCTION

Studies on a certain class of nonequilibrium systems, namely driven diffusive systems, have revealed many features that are unexpected in systems in thermal equilibrium [1–3]. For example, it is well known that although in thermal equilibrium, one-dimensional systems with short-range interaction cannot exhibit phase transition or spontaneous symmetry breaking, certain driven diffusive systems do exhibit such phenomena even in one dimension [4]. Asymmetric simple exclusion processes (ASEP), which involve biased hopping of particles in one direction, with hard-core exclusion along a one-dimensional lattice, fall in the class of driven diffusive systems and despite its simplicity, such processes are capable of exhibiting variety of phenomena [4–7]. It is the violation of detailed balance by a nonzero particle current that makes these systems so special. This, for example, is reflected in the boundary induced phase transitions in ASEP on one-dimensional finite lattice [8], where, unlike equilibrium, the effect of boundaries propagates into the bulk by a finite particle current.

In this paper, we consider a particle nonconserving version of ASEP with open boundaries. Particles, after being injected at the left boundary, hop forward with rate unity (no backward hopping is allowed) with hard-core exclusion until they reach the right boundary where they are withdrawn [9,10]. We imagine that the boundaries are coupled to particle reservoirs of constant densities. Particle injection and withdrawal rates are such that the left and right boundaries have constant densities α and γ, respectively. There is no conservation of particle in the bulk due to the possibility of attachment (detachment) of particles to (from) the lattice with a rate ω_a (ω_d). With the variation of the boundary densities, such systems exhibit different phases which are characterized by the shape of the density profiles and the nature of the current densities [9]. Mean field analysis and Monte Carlo simulations have been done in the past to find out the phase diagram for this system. The results from these analysis match remarkably well. It has been found that these systems have a rich phase diagram (see Figs. 1 and 2) compared to those without particle adsorption/desorption kinetics. For example, there is a phase where the density profile exhibits a jump from a low to a high value at some point in the bulk. This new phase, to be called a shock phase (S), appears in addition to the high-density (H) and low-density (L) phases where the bulk density, though not constant, remains above and below one-half, respectively. Although the shock phase is present for both $K=1$ and $K\neq 1$, with $K=\omega_a/\omega_d$, these two cases are distinctly different. For equal adsorption-desorption case ($K=1$), there is an additional particle-hole symmetry. This special symmetry allows a maximal current (M) phase with bulk density equal to 1/2. Furthermore, there are possibilities of coexistence of M phase with L and/or H phase (LMH, LM, and HM phases) for $K=1$. None of these is observed in the $K\neq 1$ case. These issues and also the differences in the shapes of the phase boundaries and in the nature of the phase transitions in the two cases make the problem altogether nontrivial.

In a recent work [3], Mukherji and Bhattachrjee have studied the phase transition between the low-density and shock phases using boundary layer techniques. This analysis reveals that the transition to the S phase from the L phase has a precursor of a critical deconfinement of a boundary layer near one of the open ends. In addition, this approach provides a general framework for characterizing the transitions for different values of K and also for studying different mean field models with additional interparticle interactions. The purpose of the present work is to employ the boundary layer

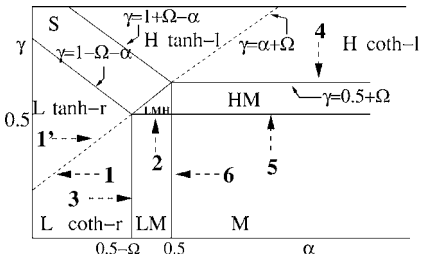

FIG. 1. Phase diagram for $K=\omega_a/\omega_d=1$ and $\Omega=\omega_d N<0.5$. N is the number of lattice points. The coexistence of a maximal-current and a low- or a high-density phase is represented by LM or HM, respectively. The coexistence of low-density, maximal-current, and high-density phases is similarly represented by LMH. Approach to different phase boundaries is indicated by the paths with arrows. Divergences, as the phase boundaries are approached along these paths, are discussed in Sec. III A, III C, and IV. "l" and "r" indicate the presence of boundary layers at left and right boundaries, respectively. Dashed lines represent the surface transition lines.

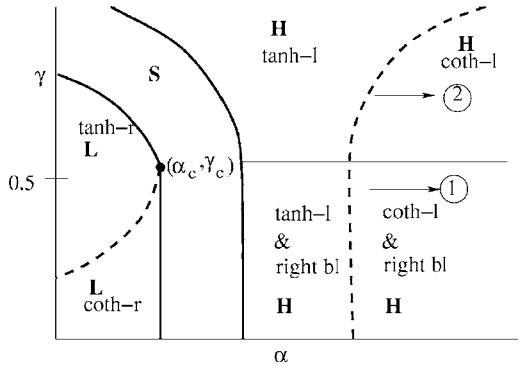

FIG. 2. Phase diagram for $K\neq 1$ and $\Omega=\omega_d N<0.5$. N represents the number of lattice points. Dashed lines represent the surface transition lines. "bl" implies boundary layer. "l" and "r" indicate the presence of boundary layers at left and right boundaries, respectively. The filled black circle represents the critical point.

theory to the mean field version of the model to understand various phase transitions from a boundary layer point of view. From this analysis, it becomes clear that the divergences of some of the length scales associated with the boundary layers also indicate bulk phase transitions. In addition, our analysis reveals the possibilities of surface transitions within the low- and high-density phases for both $K=1$ and $K\neq 1$. Except for the analysis of the surface transition, the discussion is primarily limited to $K=1$ because of several distinct phases and phase transitions (compared to $K\neq 1$).

Mean field theories provide a nonperturbative approach that is applicable in the whole parameter space. Quite often, especially in the absence of exact or rigorous solutions, mean field analysis helps in developing the qualitative picture of the phases and the phase transitions in the system. The justification for the validity or failure of the mean field analysis helps in broadening the overall understanding of the problem, as is well known from the history of equilibrium phase transitions. For the particle nonconserving ASEP problem in hand, mean field theories are known to capture the basic features [9,11]. Therefore, it is necessary to obtain the complete mean field picture of the problem, especially since no exact solution or rigorous results on nonconserving ASEP case are available.

The paper is organized as follows. The model, its symmetry properties and a few known results have been discussed in Sec. II. We discuss the boundary layer analysis for this model in Sec. III. This section is divided into three sections for the discussion of the low-density, high-density, and maximal current related phases. Since the phase boundaries, shapes of the density profiles in the low- and high-density phases depend crucially on the value of K, we divide these sections further for separate discussions on $K=1$ and $K\neq 1$. Among the maximal current related phases, we discuss mainly the LM and HM phases. Since the shape of the density profiles in the LMH and M phases can be easily understood from the knowledge of the same in the LM and HM phases, we do not discuss these phases in detail. Observations related to the behavior of the boundary layers near the phase boundaries are mentioned in Sec. IV. Finally, we conclude with a summary of our results in Sec. V. A few technical details involving the boundary layers in the maximal current phase have been mentioned in Appendix A. We provide a list of exponents and their values in Appendix B.

II. MODEL

To describe the ASEP of noninteracting single species of particles, we consider a one-dimensional chain of N lattice points and length l. Denoting the occupancy of the ith site by τ_i, which assumes values 0 or 1 depending on whether the site is empty or occupied by a particle, one may write the mean field master equation describing the time evolution of $n_i=\langle\tau_i\rangle$, with $\langle\cdots\rangle$ denoting the statistical average, as

$$\frac{dn_i}{dt}=n_{i-1}(1-n_i)-n_i(1-n_{i+1})+\omega_a(1-n_i)-\omega_d n_i. \quad (1)$$

In this equation, the mean field approximation is implemented by neglecting correlations as

$$\langle\tau_i\tau_{i+1}\rangle=\langle\tau_i\rangle\langle\tau_{i+1}\rangle. \quad (2)$$

In the large N limit, with the lattice spacing $l/N\to 0$, one can go over to the continuum by substituting $\langle\tau_{i\pm 1}\rangle=\rho(x,t)\pm\frac{1}{N}\frac{\partial\rho}{\partial x}+\frac{1}{2N^2}\frac{\partial^2\rho}{\partial x^2}\cdots$, where $\rho(x,t)$, is an average density at position $x=il/N$. The choice, $l=1$, simplifies the notation and restricts the variable x within a range $\{0,1\}$. Keeping terms up to $O(N^{-2})$, one obtains the following equation describing the shape of the density profile in the steady state:

$$\epsilon\frac{d}{dx}\left(f_2(\rho)\frac{d\rho}{dx}\right)+f_1(\rho)\frac{d\rho}{dx}+\Omega f_0(\rho)=0, \quad (3)$$

with $\Omega=\omega_d N$, $\epsilon=1/(2N)$ and $f_i(\rho)$ for $i=0,1,2$ given as follows. For the dynamics that we have considered here,

$$f_2(\rho)=1,\quad f_1(\rho)=2\rho-1,\quad f_0(\rho)=K(1-\rho)-\rho. \quad (4)$$

These f functions, in general, contain information about the dynamics. Such general form for Eq. (3) will be useful later to make certain general predictions about the boundary layers. In addition, Eq. (3) is subjected to the boundary conditions

$$\rho(x=0)=\alpha,\quad \rho(x=1)=\gamma. \quad (5)$$

The last term in Eq. (3) originates from particle adsorption-desorption kinetics and is responsible for the loss of particle number conservation in the bulk. In the absence of this term, the full equation describing the time evolution of $\rho(x,t)$, is expressible as a continuity equation

$$\frac{\partial\rho(x,t)}{\partial t}=-\frac{\partial j}{\partial x}, \quad (6)$$

with the particle current-density j given as

$$j=-\epsilon f_2(\rho)\frac{\partial\rho}{\partial x}-\hat{f}_1(\rho),\quad \text{where}\ \frac{\partial\hat{f}_1(\rho)}{\partial\rho}=f_1(\rho). \quad (7)$$

In the case of Eq. (4), the current is given by

$$j = -\epsilon\frac{\partial\rho}{\partial x} + \rho(1-\rho). \tag{8}$$

In the continuum limit ($\epsilon \to 0$), the current-density $j=\rho(1-\rho)$ is bounded, $j \leq 1/4$. Since, in the maximal current phase, the bulk density is $\rho=1/2$, the current-density acquires its maximum value, $j=1/4$, in this phase.

A. Symmetries

We now exploit the particle-hole symmetry of the problem to identify a few generic features of the problem. The hopping of a particle in the forward direction is equivalent to the hopping of a hole in the backward direction. Similarly, the injection of particles at one boundary with a certain rate is equivalent to the withdrawal of holes with the same rate. The attachment or detachment of particles can be interpreted as detachment or attachment of holes. The invariance of Eq. (3) along with f functions in Eq. (4) under the transformation

$$\rho \to 1-\rho, \quad x \to 1-x, \tag{9}$$

$$\omega_a \leftrightarrow \omega_d, \quad \alpha \leftrightarrow 1-\gamma, \tag{10}$$

implies that the particle-hole symmetry is respected by the system. This symmetry is not necessarily an obvious property of the system and can be easily destroyed by additional symmetry breaking interaction terms [3,8].

The situation with $K=1$ is somewhat special. If the adsorption-desorption kinetics were the only dynamics, the system would have settled in a steady-state density, known as the Langmuir density

$$\rho_l = K/(K+1) \tag{11}$$

determined from $f_0(\rho)=0$. If the hopping rules respect conservation, then, in the steady state, there should be a homogeneous current, if this is the only dynamics. The corresponding density ρ_c is determined from the zero of $f_1(\rho)$, i.e.,

$$f_1(\rho_c) = 0. \tag{12}$$

In case of particle-hole symmetry, we expect $\rho_c=1-\rho_c$, i.e., $\rho_c=1/2$ to be special. This, as noted earlier, is the maximal current state. If $\rho_c=\rho_l$, then $\rho=\rho_c$ becomes a particular solution of the equation. ρ_c is the density at which bulk may allow nonanalytic behavior in the density. This feature is useful for shock formation [3] though the discontinuity is rounded by the ϵ-dependent term in Eq. (3). The adsorption-desorption dynamics need not respect this symmetry of hopping and hence the two densities need not be equal. $K=1$ is a special case where the two densities become equal and the bulk dynamics is symmetric under the transformation $\rho(x) \to 1-\rho(1-x)$.

B. Known results

In addition to the knowledge about the phases, phase boundaries, the current, and the density profiles at different phases [9], we have a detailed understanding about the phase transition to the shock phase [3]. The transition to the shock phase from the low-density phase is special (e.g., for $K>1$) since the transition can be critical for certain boundary condition (α_c, γ_c) (see Fig. 2). The shock formed at the low density-shock phase boundary above the critical point has a finite height. The height of the shock on the phase boundary keeps reducing as one approaches the critical point until it becomes zero at the critical point. Below the critical point, for a fixed $\gamma \leq \gamma_c$, the height of the shock grows continuously from zero as $h \sim |\alpha-\alpha_c|^{\beta'}$ as one enters the shock phase. Associating the formation of the shock with the deconfinement of a boundary layer from the boundary of the system, it has been realized that the critical point corresponds to the divergence of a length scale related to the boundary layer [3]. This length scale, w, describes the crossover of the boundary density to the bulk and diverges as $w \sim |\alpha-\alpha_c|^{\zeta_c}$ for $\gamma=\gamma_c$ and $\alpha \to \alpha_c-$. It has been found that $\zeta_c=1,1/2$ for $K=1$ and $K \neq 1$, respectively. Further quantitative description of the transition regarding the shape of the phase boundary near the critical point, the variation of the height of the shock as the critical point is approached along the phase boundary, the exponent β' are available in Ref. [3]. These derivations depend on a few general properties of the dynamics without relying on specific details.

III. BOUNDARY LAYER ANALYSIS

By changing the boundary values α and γ, one may map out all possible steady state configurations, thereby constituting a "phase diagram" of the nonequilibrium system in the $N \to \infty$ limit. To understand all these phases, we use a leading order boundary layer analysis that provides a systematic way to generate a uniform approximation of the solution of Eq. (3). In all the phases, the density profile over almost the entire space, is described by the solution of the first order equation obtained by ignoring the second derivative term $(\epsilon \to 0)$ in Eq. (3). This solution, known as the outer solution, is not, in general, expected to satisfy both the boundary conditions. In order to satisfy the boundary conditions appropriately, there appear special regions with boundary layers or shocks. A description of these special regions requires going beyond the first order equation. The solutions describing the boundary layers or shocks are known as inner solutions. The constants in different solutions of the differential equations are determined either by the boundary conditions or by smooth joining of the inner and outer solutions.

The low- and high-density phases are related to each other due to particle-hole symmetry and does not require any separate treatment. The difference between the low-density and the maximal current phase arises from the outer solution itself. The outer solutions, solutions of the first order equation [Eq. (3) in the limit $\epsilon \to 0$], are

$$\rho_{1,\text{out}} = 1/2, \quad \rho_{2,\text{out}} = \Omega x + c, \quad \text{for } K=1, \tag{13}$$

$$\Omega x = g(\rho_{\text{out}}) - c, \tag{14}$$

with

$$g(\rho) = \frac{1}{1+K}\left(2\rho + \frac{K-1}{K+1}\ln[K-(1+K)\rho]\right) \quad \text{for } K \neq 1. \tag{15}$$

Here, c is an unknown constant to be determined from the boundary condition. In the low- and high-density phases, the density profile, over almost the entire space, is described by the linear solution in Eq. (13) for $K=1$ or by the solution in Eqs. (14) and (15) for $K \neq 1$. The maximal current phase, present only for $K=1$, has a constant density profile described by the outer solution $\rho_{1,\text{out}}$. In the phase diagram for $K=1$, there are other regions with coexistence of the maximal current phase with low- or high-density phases or both. The density profile in these phases has constant part $\rho_{1,\text{out}}(x)=1/2$ as well as linear parts $\rho_{2,\text{out}}=\Omega x+c$ with different parts connected continuously through specific inner solutions.

The scheme to find the inner solution varies depending upon the kind of matching conditions the inner solution must satisfy. The procedure to find out the inner solution for L/H phases is different from that for phases involving M phase. The difference arises because in the latter case, the inner solutions are required to saturate to $\rho(x)=1/2$ at either of the two sides and at this value of ρ, $f_1(\rho)=0$. In the low- or high-density phases, the boundary layer is not required to saturate to $1/2$. Because of these differences, we discuss L, H, and M-related phases in different sections.

A. Surface transition in the low-density phase: A general analysis

In the low-density phase, $c=\alpha$ for $K=1$ and $c=g(\alpha)$ for $K \neq 1$, since the outer solution satisfies the left boundary condition. To find the inner solution, one needs to express Eq. (3) in terms of $\tilde{x}=(x-x_d)/\epsilon$, where x_d, which, at present, is arbitrary, specifies the location of the solution after the implementation of the boundary conditions. In the $\epsilon \to 0$ limit, the contribution from the Ω-dependent term can be ignored. Using the definition of $\hat{f}_1(\rho)$ in Eq. (7), we may write the inner solution as the solution of the equation

$$f_2(\rho_{\text{in}})\frac{d\rho_{\text{in}}}{d\tilde{x}} + \hat{f}_1(\rho_{\text{in}}) = \text{const}. \tag{16}$$

Incorporating the matching condition, $\rho_{\text{in}}(\tilde{x}\to-\infty)=\rho_o \equiv \rho_{2,\text{out}}(x=1)$ for smooth joining of the inner and the outer solutions, we may re-express this equation as

$$\frac{d\rho_{\text{in}}}{d\tilde{x}} = \frac{F(\rho_{\text{in}})}{f_2(\rho_{\text{in}})}, \tag{17}$$

where

$$F(\rho) \equiv \hat{f}_1(\rho_o) - \hat{f}_1(\rho). \tag{18}$$

The inner region obeys the particle conservation condition and the continuity equation demands a homogeneous current. Consequently, the current must be equal to the bulk current entering the region. This is the content of Eqs. (17) and (18) though derived in a different way. It is important to know that although the inner solution is obtained from the Ω-independent part of Eq. (3), the effect of particle nonconservation enters in the inner solution through the matching condition where ρ_o is a function of Ω.

The condition for saturation of the inner solution as $\tilde{x}\to\infty$ requires

$$F(\rho) = 0 \quad \text{for } \rho = \rho_s > \rho_o. \tag{19}$$

If $\gamma > \rho_{\text{in}}(\tilde{x}\to\infty)$, the boundary condition cannot be satisfied by ρ_{in}. As a result, the surface layer deconfines from the surface and enters into the bulk with the outer solution again appearing at the right edge to satisfy the right boundary condition. This mechanism leads to the formation of a shock in the density profile at the bulk. The bulk transition to the shock phase, therefore, has a precursor of deconfinement of the surface layer. Since ρ_o is a function of α, one has a phase boundary on the α-γ plane $\gamma=\rho_s((\rho_o(\alpha))$ that separates the low-density phase from the shock phase. With $f_1(\rho)=2\rho-1$, we have $\hat{f}_1(\rho)=\rho^2-\rho+\text{constant}$. Substituting this in Eq. (18), we find $\rho_s=1-\rho_o$. Assuming simple zeros for $F(\rho)$, we write

$$F(\rho) = -(\rho-\rho_o)(\rho-\rho_s)\phi(\rho), \tag{20}$$

where $\phi(\rho)$, in general, takes care of any multiplicative prefactor. For the set of f-functions given in Eq. (4), $\phi(\rho)=1$. This form of $F(\rho)$ is convenient as it yields the length scale associated with the crossover of the surface profile to the bulk profile quite generally. The large $\tilde{x}$ behavior of the inner solution can be found from

$$\frac{d\rho_{\text{in}}}{d\tilde{x}} \sim -\frac{(\rho_{\text{in}}-\rho_s)}{w(\alpha)}, \tag{21}$$

where

$$w(\alpha) = (\rho_s-\rho_o)^{-1}\frac{f_2(\rho_s)}{\phi(\rho_s)}. \tag{22}$$

We have used $\rho_{\text{in}} \approx \rho_s$ to obtain Eq. (21). Equation (21) shows $w(\alpha)$ as the characteristic length scale for the approach to saturation or to the bulk density. $w(\alpha)$ can be made to diverge by changing α and this locates a critical point on the phase boundary between the low-density and the shock phase. At this critical point (α_c, γ_c), $\rho_s=\rho_o=\gamma_c$.

Given this form of $F(\rho)$, in the low-density phase, the slope of the inner solution at $x=1$, i.e., at $\rho=\gamma$, is positive if $\rho_o<\gamma<\rho_s$ and negative if $\gamma<\rho_o$. Thus, with $\gamma_{\text{sc}}=\rho_o$, there is an increasing solution at $x=1$ for $\gamma>\gamma_{\text{sc}}$ and a decreasing one for $\gamma<\gamma_{\text{sc}}$. This leads to a general conclusion, that for every α, if there is a bulk transition at $\gamma=\rho_s((\rho_o(\alpha))$, there is a "boundary" transition at $\gamma=\rho_o(\alpha)$. This defines a surface transition line in the low-density phase. The transition is strictly at the boundary because as one crosses the phase boundary, the bulk density profile remains the same but the boundary profile changes drastically. Such surface transition is expected to be true generally for all K and also for the interacting system, wherever a transition to a shock phase takes place.

The solution of the first order equation (17), involves a constant which we denote by ξ. In terms of the natural length

scale set by Eq. (17) and the constant ξ, the inner solution, in general, can be written as

$$\rho_{\rm in}(\tilde{x}) = \rho_{\rm o} S_{\rm in}(\tilde{x}/2w + \xi), \tag{23}$$

with $S_{\rm in} \to 1$ as $\tilde{x} \to -\infty$. The constant, ξ, can be determined from the constraint $S_{\rm in}(\tilde{x}=0)=\gamma$ and the explicit form of $F(\rho)$ specified in Eq. (20). Near the surface transition line, ξ has a logarithmic divergence

$$\xi \sim \ln|\gamma - \rho_o(\alpha)|. \tag{24}$$

This implies that for a given γ, the surface transition takes place at $\alpha=\alpha_{\rm surf}(\gamma)$ with

$$\xi \sim |\alpha - \alpha_{\rm surf}|^{-\zeta_s}. \tag{25}$$

Since in our case, the divergence of ξ is logarithmic,

$$\zeta_{\rm s} = 0 \ (\ln) \tag{26}$$

in the notation of power law. These predictions of the exponents are general and based on a few generic properties of the dynamics. In the following we illustrate this general approach for special cases of $K=1$ and $K \neq 1$.

Results for $K=1$ *and* $K \neq 1$: Following the above arguments, surface transition lines can be obtained for all values of K. For all K, the explicit inner solution with positive slope at $x=1$ is

$$\rho_{\rm in}(\tilde{x}) = \frac{1}{2} + \frac{(1-2\rho_o)}{2} \tanh\left(\frac{\tilde{x}}{2w} + \xi\right), \tag{27}$$

where ξ is a constant and

$$w = 1/(1-2\rho_o). \tag{28}$$

This solution appears for $\gamma > \rho_o$.

As $\tilde{x} \to \infty$, the inner solution saturates to $\rho_s = 1-\rho_o$. The bulk transition to the shock phase occurs when the saturation value, ρ_s, of the surface layer, is smaller than γ. The phase boundary between the low-density and the shock phase is, therefore, given by the equation $1-\rho_o(\alpha)=\gamma$. The surface transition to a boundary layer of negative slope occurs when $\gamma < \gamma_{\rm sc} = \rho_o$. The boundary layer, in this case is

$$\rho = \frac{1}{2} + \frac{1-2\rho_o}{2} \coth\left(\frac{\tilde{x}}{2w} + \xi\right), \tag{29}$$

where w is the same as in Eq. (28). w and ξ together determine the position of the "virtual origin" at which the argument of the inner solution vanishes. This is simply in the sense of mathematical continuation since the virtual origin may lie well beyond the physical range of x, $\{0,1\}$, with an unphysical value of the density.

For $K=1$, using $\rho_o = \Omega + \alpha$, we find

$$w = 1/(1-2\Omega-2\alpha). \tag{30}$$

Further, the constraint $\rho_{\rm in}(\tilde{x}=0)=\gamma$, leads to

$$\xi = \frac{1}{2} \ln\left(\frac{\gamma - \Omega - \alpha}{1-\Omega-\alpha-\gamma}\right), \tag{31}$$

for tanh type boundary layer (see Fig. 3) and

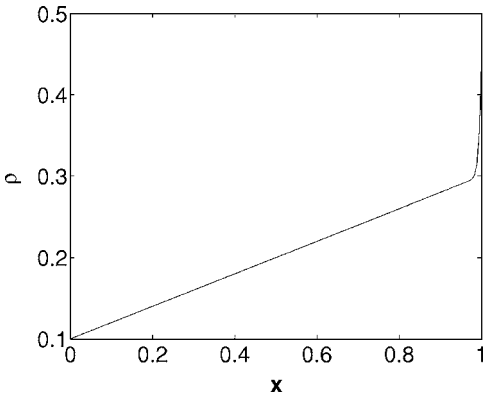

FIG. 3. Density profile with positive slope at the right boundary for $K=1$ with $\alpha=0.1$, $\gamma=0.44$, $\epsilon=0.0035$, and $\Omega=0.2$.

$$\xi = \frac{1}{2} \ln\left(\frac{\gamma - (\Omega+\alpha)}{\gamma - (1-\Omega-\alpha)}\right) \tag{32}$$

for coth boundary layer (see Fig. 4). The surface transition from the tanh type boundary layer to the coth type boundary layer takes place if $\gamma < \gamma_{\rm sc} = \rho_{\rm o} = \Omega + \alpha$ leading to a linear surface transition line, $\gamma = \Omega + \alpha$, on the α-γ plane (see Fig. 1). As this line is approached from either of the two low-density phases [along path (1) or (1′) in Fig. 1], ξ diverges logarithmically as

$$\xi \sim \ln|\gamma - \Omega - \alpha|. \tag{33}$$

The surface transition line $\rho_o(\alpha)=\gamma$ and the shock phase boundary $\rho_{\rm s}=1-\rho_o(\alpha)=\gamma$ intersect at $\rho_{\rm o}=1/2$. This intersection point is, therefore, also the critical point (α_c, γ_c) at which $w(\alpha)$ diverges. For $K=1$, the critical point is $(1/2-\Omega, 1/2)$. For $\gamma < \gamma_c$, this boundary layer with negative slope at $x=1$ cannot produce shock through deconfinement from the boundary layer if α is increased. As α is increased, this decaying boundary layer instead maintains its decaying profile in the low-density maximal-current (LM) phase.

For $K \neq 1$, ρ_o is the solution of $g(\rho_o)=\Omega+g(\alpha)$ with $g(\rho)$ given in Eq. (15). In this case, therefore, the surface transition line $\gamma=\gamma_{\rm sc}=\rho_o$ is determined from the solution for γ from the equation

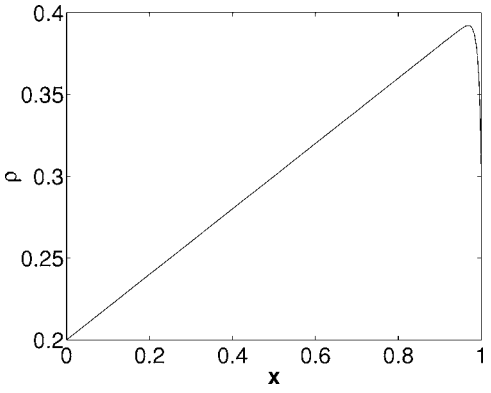

FIG. 4. Density profile with negative slope at the right boundary for $K=1$ with $\alpha=0.2$, $\gamma=0.3$, $\epsilon=0.0035$, and $\Omega=0.2$.

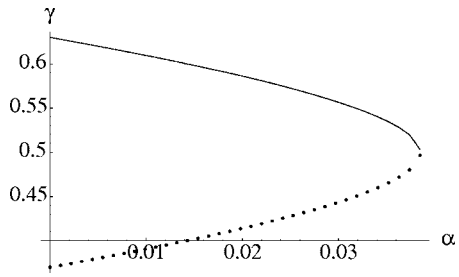

FIG. 5. Dotted line represents the surface transition line in the low-density phase for $K=3$ and $\Omega=0.1$. The solid line corresponds to the phase boundary between the low-density and the shock phase. The intersection of the two lines is the critical point (α_c, γ_c).

$$g(\gamma) = \Omega + g(\alpha). \tag{34}$$

The condition for shock formation from a low-density phase with tanh type boundary layer, on the other hand, leads to a phase boundary given by the solution of the equation

$$g(1-\gamma) = \Omega + g(\alpha). \tag{35}$$

The solutions for γ from Eqs. (34) and (35) are symmetric around $\gamma=1/2$ (see Fig. 5) and the intersection of the two solutions at $\gamma=\gamma_c=1/2$ is the critical point (α_c, γ_c) (see also Fig. 2) where

$$g(\gamma_c) = \Omega + g(\alpha_c). \tag{36}$$

Since the surface transition line is symmetric to the phase boundary between the shock and the low-density phases, shapes of these two lines close to the critical point are the same [3]. The shape of the surface transition line can be obtained independently by substituting $\gamma=\gamma_c-\Delta\gamma$ and $\alpha=\alpha_c-\Delta\alpha$ in Eq. (34) and expanding it in small $\Delta\gamma$ and $\Delta\alpha$. This leads to a general equation

$$g'(\gamma_c)\Delta\gamma - g''(\gamma_c)(\Delta\gamma)^2/2 + \cdots = g'(\alpha_c)\Delta\alpha. \tag{37}$$

Since for $K\neq 1$, $g'(\gamma_c)=0$, the shape of the surface transition line near the critical point is given by

$$\Delta\gamma \sim |\Delta\alpha|^{\chi_-^s} \quad \text{with } \chi_-^s = 1/2. \tag{38}$$

For $K=1$, the surface transition line, $\gamma=\Omega+\alpha$, being linear in γ and α leads to

$$\chi_-^s = 1. \tag{39}$$

The same set of boundary layers for $K\neq 1$, however, gives rise to a logarithmic divergence of ξ across the surface transition line. Similar to the $K=1$ case, the coth boundary layer, in the low-density phase, leads the way to a decaying boundary layer in the shock phase for $\gamma<\gamma_c$.

The mechanism for the formation of the shock for $\gamma>\gamma_c$, is different from that for $\gamma<\gamma_c$, since in the latter case, there is no tanh type boundary layer to be deconfined to form a shock. The effective boundary condition for shock formation, for $\gamma<\gamma_c$ is the same as $\gamma=\gamma_c$ since the right branch of the outer solution satisfies this effective boundary condition at its right edge. The original boundary condition $\rho(x=1)=\gamma$ with $\gamma<\gamma_c$ is satisfied finally with a decaying boundary layer. As a consequence of this, α_c continues to be the critical value of α for shock formation for all $\gamma<\gamma_c$ leading to a vertical phase boundary between the low-density and the shock phase (see Fig. 2). As α increases in the shock phase, the discontinuity, formed at $x=1$, moves toward $x=0$ until it reaches the other end at the high-density-shock phase-boundary. Whereas for $\gamma>\gamma_c$, the deconfined boundary layer or the shock at $x=1$ has a finite height, for $\gamma<\gamma_c$, the shock height increases continuously from zero to a finite value as α is increased. Although the mechanism of shock formation is different for $\gamma>\gamma_c$ and $\gamma<\gamma_c$, the discontinuity is always described by a tanh type inner solution. Alternatively, for all values of γ, the emergence of shock, as one approaches the shock phase from the high-density side, is through the deconfinement of a tanh boundary layer of finite height at $x=0$. As a consequence of this, the high-density shock phase boundary cannot have any critical point on it.

The entire process of the surface transition and, then, the shock formation by changing γ for a given α can be understood on a more physical ground. In the low-density phase, for small γ, the withdrawal rate at $x=1$ is high. Since the bulk dynamics is completely controlled by hopping and adsorption-desorption kinetics, a large withdrawal rate with a fixed α, causes particle depletion at $x=1$ to be described by a "virtual origin" somewhere at $x>1$. As γ is increased, the withdrawal rate decreases and we reach a situation where there is neither any depletion nor any accumulation of particles at the end. The "virtual origin" is shifted to ∞ now. If γ is increased further, the withdrawal rate is too slow to get rid of the particles that reach the open end. This leads to an accumulated region at the boundary until a stage where this accumulated region becomes macroscopic. Beyond this point, the withdrawal rate controls the density near the end and the injection rate controls the remaining part of the density with the two parts joined through a shock or discontinuity.

B. High-density phase

1. $K=1$

For $K=1$, the H phase can be completely understood from the knowledge about the L phase by exploiting the particle-hole symmetry. In this sense, the high-density phase for particles is equivalent to the low-density phase for holes with density profile the same as that in Fig. 3 or Fig. 4 when the coordinates are transformed as $x\to 1-x$. In this transformed coordinates, above the line $\gamma=\Omega+\alpha$, we have the density profile for holes the same as in Fig. 3. The boundary layer here is described by Eq. (27) with the constants

$$w = 1/(2\gamma - 2\Omega - 1), \tag{40}$$

$$\xi = \frac{1}{2}\ln[(\gamma-\Omega-\alpha)/(\gamma+\alpha-1-\Omega)]. \tag{41}$$

It is straightforward to verify that the particle density profile in the original coordinates is as shown in Fig. 6. It consists of a linear profile satisfying the right boundary condition and a boundary layer as in Eq. (27) with

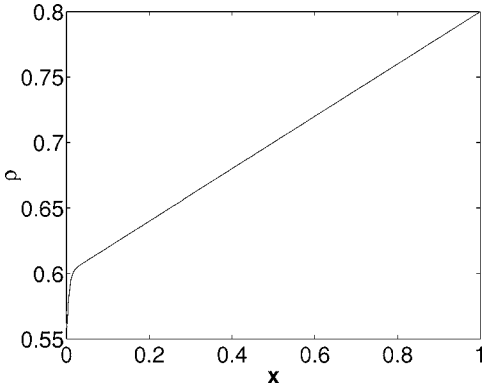

FIG. 6. Density profile with positive slope at the left boundary for $K=1$ with $\alpha=0.55$, $\gamma=0.8$, $\epsilon=0.002$ and $\Omega=0.2$.

$$\xi = \frac{1}{2}\ln[(\gamma+\alpha-1-\Omega)/(\gamma-\Omega-\alpha)], \tag{42}$$

and w is the same as in (40). The particle-hole symmetry also guarantees a surface phase transition in the high-density phase across $\gamma=\Omega+\alpha$ line. The tanh type boundary layer at $x=0$ with positive slope changes to a boundary layer with negative slope (see Fig. 7) described by Eq. (29) with constants that can be determined using the symmetry.

2. $K \neq 1$

The high-density phase can be divided into two major parts. For $\gamma<\gamma_c=1/2$, the density profile has boundary layers on both the ends. In addition to a tanh type boundary layer at $x=0$, there is a decaying boundary layer at $x=1$. The right boundary layer helps the density profile satisfy the boundary condition at $x=1$ from a value $\rho=1/2$. Thus as in the case of shock phase with $\gamma<1/2$, the effective boundary condition on the right edge for the outer solution continues to be $\rho=1/2$ in this part of the H phase. In the other part of the H phase, the density profile has only one tanh boundary layer at $x=0$.

The transition to the shock phase from the high-density phase takes place through the deconfinement of the inner solution

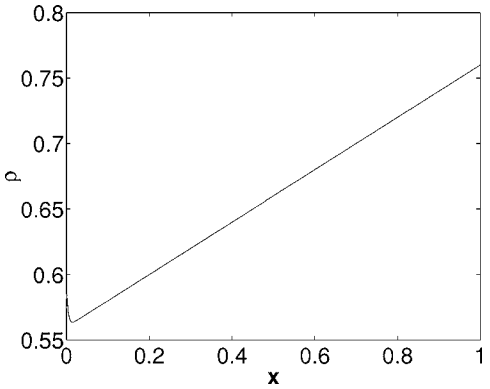

FIG. 7. Density profile with negative slope at the left boundary for $K=1$ with $\alpha=0.6$, $\gamma=0.76$, $\epsilon=0.001$, and $\Omega=0.2$.

$$\rho = 1/2 + \frac{(2\rho_o'-1)}{2}\tanh\left(\frac{(2\rho_o'-1)\tilde{x}}{2}+\xi\right), \tag{43}$$

at $x=0$. Here $\rho_o'=\rho_{\text{out}}(x=0)$ is the value of the outer solution at $x=0$. For $\gamma>1/2$, the outer solution obeying the boundary condition $\rho(x=1)=\gamma$ can be obtained by solving

$$g(\rho_o') = -\Omega + g(\gamma). \tag{44}$$

For $\gamma<1/2$, the outer solution satisfies the effective boundary condition $\rho(x=1)=1/2$ and it is the solution of the equation

$$g(\rho_o') = -\Omega + g(1/2). \tag{45}$$

The boundary layer deconfines, whenever α is smaller than $1-\rho_o'$, the saturation value of the inner solution in Eq. (43). This leads to the high-density-shock phase boundaries,

$$g(1-\alpha) = -\Omega + g(1/2) \quad \text{for } \gamma<1/2, \tag{46}$$

$$g(1-\alpha) = -\Omega + g(\gamma) \quad \text{for } \gamma>1/2. \tag{47}$$

Since for $\gamma<1/2$, the value of the critical α does not depend on γ, the phase boundary is vertical for all $\gamma<1/2$, with a K dependent value of α.

Across the surface transition line, the slope of the boundary layer at $x=0$ changes sign. If the value of ρ_o' is larger than α, a boundary layer with a positive slope at $x=0$ is expected. In the reverse situation, one expects a boundary layer with a negative slope at $x=0$. The transition lines are, therefore, given by

$$g(\alpha) = -\Omega + g(1/2) \quad \text{for } \gamma<1/2, \tag{48}$$

$$g(\alpha) = -\Omega + g(\gamma) \quad \text{for } \gamma>1/2. \tag{49}$$

The surface transition lines in Eqs. (48) and (49) are represented by dashed lines 1 and 2, respectively, in Fig. 2. These two lines meet at $\gamma=1/2$ with a value of α that depends on K. The surface transitions across both the lines are associated with the divergence of ξ and there is no critical point on these lines.

C. Boundary layers in *LM* and *HM* phases for $K=1$

For $K=1$, $\alpha=1/2-\Omega$ and $\gamma=1/2+\Omega$ are the boundaries for the low-density and high-density phases, respectively, since tanh or coth type boundary layers are no longer valid on these lines. The *LM* phase and the symmetrically opposite *HM* phase appear in the regimes $\{1/2-\Omega<\alpha<1/2, \gamma<1/2\}$ and $\{\alpha>1/2, 1/2<\gamma<1/2+\Omega\}$, respectively. In the *LM* phase (see Fig. 8), the linear profile, $\rho(x)=\Omega x+\alpha$, satisfies the left boundary condition and continues until $x_{\text{cl}}=(1/2-\alpha)/\Omega$ where $\rho(x_{\text{cl}})=1/2$. The constant profile continues until the other end where a boundary layer finally satisfies the boundary condition. In the *HM* phase (see Fig. 9), the linear profile satisfying the right boundary condition ends at $x_{\text{ch}}=(1-2\gamma+2\Omega)/2\Omega$ with constant density profile for $x<x_{\text{ch}}$ and a boundary layer at $x=0$. To obtain the boundary layer near $x=1$ (or $x=0$) for *LM* (or *HM*) phase, it is useful to express Eq. (3) in terms of

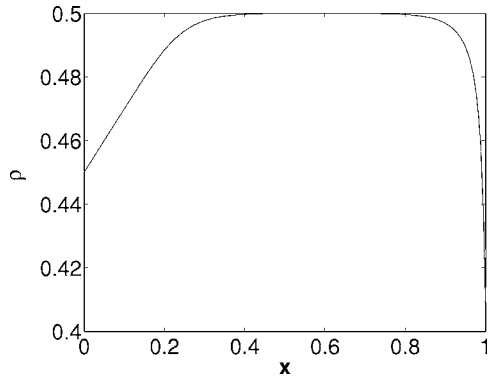

FIG. 8. Density profile in the low-density maximal current (LM) phase with $\alpha=0.45$, $\gamma=0.4$, $\epsilon=0.002$ and $\Omega=0.2$.

$$f(x^*) = (2\rho - 1)/\sqrt{\epsilon}, \tag{50}$$

with $x^* = (x - x_0)/\sqrt{\epsilon}$, where x_0, as before, represents the center of the solution. In terms of $f(x^*)$, the equation is

$$\frac{1}{2}\frac{\partial^2 f}{\partial x^{*2}} + \frac{f}{2}\frac{\partial f}{\partial x^*} - \Omega f = 0. \tag{51}$$

A phase plane analysis [12] of Eq. (51) is useful to identify the appropriate inner solution that can satisfy the boundary conditions. Denoting $\frac{df}{dx^*} = p$, we have

$$\frac{dp}{df} = f\frac{2\Omega - p}{p}. \tag{52}$$

The contour plots in the p-f plane are shown in Fig. 10 which shows the contours connecting different possible boundary conditions. Some details on this are given in Appendix A.

To obtain the boundary layer at $x=1$ for the LM phase, we require the specific solution which satisfies the boundary conditions $\rho(x^*)=1/2$, as $x^* \to -\infty$ and $\rho(x^*)=\gamma$ as $x \to 1$. These conditions are fulfilled by the contour marked with a horizontal arrow in Fig. 10. The origin ($f=p=0$) is a fixed point for the differential equations and a simple linearization around this fixed point leads to $p=(2\Omega)^{1/2}f$. The approach to $\rho=1/2$ as $x^* \to -\infty$ is, therefore, exponential as

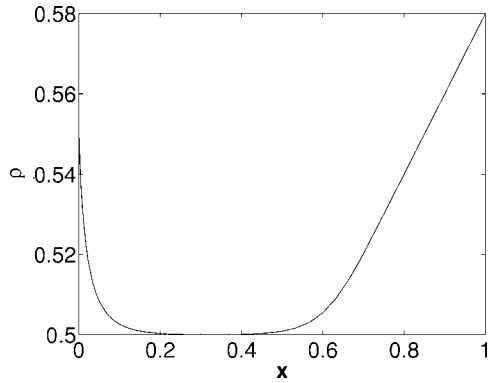

FIG. 9. Density profile in the high-density maximal current (HM) phase with $\alpha=0.55$, $\gamma=0.58$, $\epsilon=0.002$, and $\Omega=0.2$.

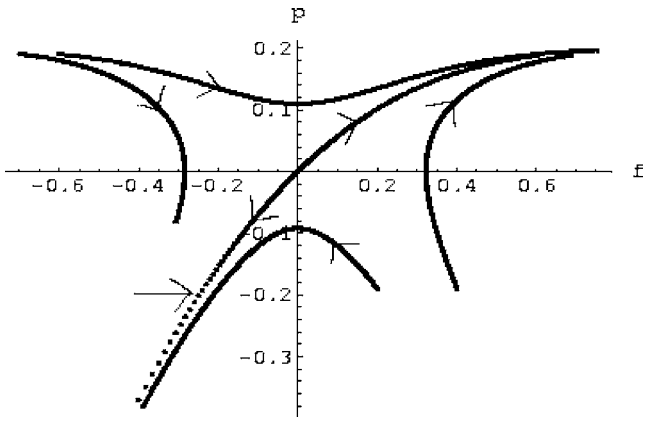

FIG. 10. Contour plots in the p-f plane for $\Omega=0.1$. The arrows on different contours indicate the directions of increasing x^*.

$$f \sim \exp[(2\Omega)^{1/2}x^*]. \tag{53}$$

Away from the fixed point ($f=p=0$), the solution of the differential equation is $f^2 \sim -2p$, implying $f \sim 2/x^*$, as $x^* \to 0$. The boundary condition $\rho(x=1)=\gamma$ further leads to $x_0 = 1 - \frac{2\epsilon}{2\gamma-1}$. As $x \to 1$, the density profile thus has an algebraic decay as

$$\rho(x) = \frac{1}{2} + \frac{\epsilon}{x - x_0} = \frac{1}{2} + \frac{\epsilon}{x - 1 + 2\epsilon/(2\gamma - 1)}. \tag{54}$$

The divergence of the scale x_0, as the boundary for the LMH phase, $\gamma=\gamma_c=1/2$, is approached from the LM side [along path (2) in Fig. 1] can be written as $x_0 \sim (\gamma_c - \gamma)^{-\zeta_1^{lm}}$ as $\gamma \to \gamma_c-$ with

$$\zeta_1^{lm} = 1. \tag{55}$$

For the HM phase, the boundary layer at the left edge must be described by the specific solution that satisfies the boundary condition at $x=0$ and approaches $\rho(x^*)=1/2$ exponentially as $x^* \to \infty$. It can be shown that this solution is the same as (54) near $x=0$, with $x_0 = \frac{2\epsilon}{1-2\alpha}$. This allows us to introduce an exponent ζ_1^{hm}, similar to that in Eq. (55), describing approach to $\alpha=1/2$ from the HM phase. Our calculation shows

$$\zeta_1^{hm} = 1. \tag{56}$$

The matching between the linear and the constant profile around x_{cl} or x_{ch} can also be done by choosing the appropriate solution from the contour plot. In the case of LM phase, this solution should merge to the linear one for $x^* \to -\infty$ and, approach 0 exponentially as $x^* \to \infty$, with the same length scale as in Eq. (53). Similar analysis is suitable also for the maximal current (M) phase, that appears for $\alpha > 1/2$ and $\gamma < 1/2$. In this phase, the density profile is fixed at $1/2$ over the entire lattice except for decaying boundary layers same as those in LM and HM phases at $x=1$ and $x=0$, respectively. In the LMH phase, there are two linear parts in the density profile satisfying the left and right boundary conditions similar to LM and HM phases, respectively. Between these two linear regimes, there is a constant regime with $\rho = 1/2$. The inner solutions that join the linear and the constant parts of the density profile are the same as those present

in the *LM* and *HM* phases. Since these inner solutions and associated divergences can be obtained following a similar analysis as above, we do not discuss these anymore.

IV. APPROACH TO VARIOUS PHASE BOUNDARIES

Our final aim is to study the boundary layers for $K=1$ as different phase boundaries are approached. As the phase boundary $\alpha=1/2-\Omega$ is approached from the low-density side (along path 3 in Fig. 1), $w\xi$ approaches a finite value $1/(2\gamma-1)$ which diverges as the special point $\gamma=1/2$ is approached. Since at this special point, $\Omega+\alpha=\gamma=1/2$, the linear profile satisfies both the boundary conditions and there is no need of any boundary layer. Since $\coth x \sim 1/x$ as $x\to 0$, there is an algebraically decaying inner solution

$$\rho(x) = \frac{1}{2} + \frac{\epsilon}{x - 1 + 2\epsilon/(2\gamma - 1)}, \tag{57}$$

near the phase boundary $\alpha=1/2-\Omega$ for $\gamma<\gamma_c$ as $x\to 1-\frac{2\epsilon}{2\gamma-1}$. This decay is exactly the same as that found in the density profile in Eq. (54) that describes the boundary layer in the *LM* phase (on the other side of the phase boundary, $\alpha=1/2-\Omega$). From this analysis, it becomes clear, how the coth boundary layer transforms to an algebraically decaying boundary layer appropriate for *LM* phase across the phase boundary. As $\tilde{x}\to-\infty$, the coth inner solution in the *L*-phase approaches $\rho_o=\Omega+\alpha$ exponentially as

$$\rho(\tilde{x}) = \Omega + \alpha - (1 - 2\Omega - 2\alpha)e^{2(\tilde{x}/2L_l+\xi)}, \tag{58}$$

with a length scale $L_l=1/(1-2\Omega-2\alpha)$ that diverges as the phase boundary $\alpha=\alpha_{lc}=1/2-\Omega$ is approached from below. We describe this divergence as $L_l \sim (\alpha_{lc}-\alpha)^{-\zeta_2^l}$ with

$$\zeta_2^l = 1. \tag{59}$$

It is interesting to note that as the phase boundary is approached, the algebraic decay of the inner solution near $x=1$ is same in both *L* and *LM* phases. The approach of the two inner solutions in *L* and *LM* phases to the bulk density, on the other hand, is exponential with two different length scales. The situation is symmetric as one approaches the *HM* and *H* phase boundary. As the phase boundary $\alpha>1/2$ and $\gamma=1/2+\Omega$ is approached from the *H* phase [along path (4) in Fig. 1], ξw in the coth boundary layer at $x=0$ approaches $1/(2\alpha-1)$. The power-law decay of the boundary layer near $x=0$ as

$$\rho(x) = \frac{1}{2} + \frac{\epsilon}{x - 2\epsilon/(1 - 2\alpha)} \tag{60}$$

is the same as that for the boundary layer in *HM* phase. The approach of the coth boundary layer to the bulk value involves a length scale L_h analogous to L_l. This, by symmetry, diverges as the phase boundary $\gamma=1/2+\Omega$ is approached from the *H* side with a similar exponent

$$\zeta_2^h = 1. \tag{61}$$

As the *HM* or *LM* phases are approached from the *M* phase, the boundary layer at $x=1$ or at $x=0$, respectively, disappears and a linear profile at the respective edge starts appearing. This is marked by the divergences of x_0 as $(1-2\gamma)^{-1}$ or $(1-2\alpha)^{-1}$ along path (5) or (6) of Fig. 1, respectively. We introduce two more exponents ζ_1^m and ζ_2^m as $x_0 \sim (\gamma_c-\gamma)^{-\zeta_1^m}$ when $\gamma\to\gamma_c$ along path 5 and $x_0 \sim (\alpha_{mc}-\alpha)^{-\zeta_2^m}$ when $\alpha\to\alpha_{mc}=1/2$ along path 6. We find

$$\zeta_1^m = \zeta_2^m = 1. \tag{62}$$

All the exponents introduced in various sections have been listed in Appendix B.

V. SUMMARY

We have studied an asymmetric simple exclusion process on an open one-dimensional lattice. The particles, after being injected at a certain rate at one end of the lattice, perform hopping in the forward direction respecting mutual exclusion. They are withdrawn at a certain rate when they reach the other end of the lattice. The injection and withdrawal rates and the density of the particle reservoirs at the boundaries are such that the system has fixed particle densities α and β at the boundaries. The particle number at the bulk is not conserved since at the bulk, there are possibilities of attachment and detachment of particles to and from the chain at certain rates. The particles in the asymmetric simple exclusion processes are analogous to the processive motor proteins that participate in the intracellular transport processes on cytoskeletal filaments. The adsorption and desorption of the particles is similar to the binding and unbinding of the motor proteins to and from the filaments. The combined effect of hopping dynamics and particle adsorption-desorption dynamics has interesting consequences on the stationary state phase diagram on α-β plane in comparison to the particle conserving asymmetric simple exclusion processes. A particularly interesting feature is that there is an extended region in the phase diagram where the density profile has a jump discontinuity from a low value to a high value. This phase is known as the shock phase. The particle adsorption and desorption kinetics here play a special role in localizing the shock which has a fluctuating position in particle conserving models. A boundary layer analysis gives an intuitive as well as a quantitative understanding as how the system enters into the shock phase from a low-density phase [3]. It has been shown in an earlier work that the shock appears into the bulk due to a deconfinement of the boundary layer from the boundary of the system. The deconfinement can become critical under certain boundary condition (α_c, γ_c). The boundary layer analysis is found to be useful for characterizing the phase transition near and away from the critical point.

The present work is aimed at understanding what role the boundary layers play when the system undergoes other bulk phase transitions. Our results are based on the boundary layer analysis on the continuum mean field equation for the steady state density profile. This analysis is asymptotic in $1/N$ and if necessary, can be extended to higher orders in $1/N$.

We have shown that the bulk phase transitions in this model are associated with divergences of certain length

TABLE I. Exponents obtained in the text.

Symbol	Description	Definition	Value
ζ_s	Divergence of ξ near the surface transition	$\xi \sim \lvert\alpha-\alpha_{\text{surf}}\rvert^{-\zeta_s}$	0 (ln)
χ_-^S	Shape of the surface transition line near the critical point	$\Delta\gamma \sim \Delta\alpha^{\chi_-^S}$	1/2 or 1
ζ_1^{lm}	Divergence of x_0 as $\gamma \to \gamma_c$ from the LM phase	$x_0 \sim (\gamma_c-\gamma)^{-\zeta_1^{lm}}$ as $\gamma \to \gamma_c-$	1
ζ_1^{hm}	Divergence of x_0 as $\alpha \to 1/2$ from the HM phase	$x_0 \sim (1/2-\alpha)^{-\zeta_1^{hm}}$ as $\alpha \to 1/2+$	1
ζ_2^l	Divergence of the length scale L_l as $\alpha \to \alpha_{lc}$ from the L phase	$L_l \sim (\alpha_{lc}-\alpha)^{-\zeta_2^l}$ as $\alpha \to \alpha_{lc}-$	1
ζ_2^h	Divergence of L_h as $\gamma \to \gamma_{hc}$ from the H phase	$L_h \sim (\gamma_{hc}-\gamma)^{-\zeta_2^h}$ as $\gamma \to \gamma_{hc}+$	1
ζ_1^m	Divergence of x_0 as $\gamma \to \gamma_c=1/2$ from the M phase	$x_0 \sim (\gamma_c-\gamma)^{-\zeta_1^m}$ as $\gamma \to \gamma_c-$	1
ζ_2^m	Divergence of x_0 as $\alpha \to \alpha_{mc}$ from the M phase	$x_0 \sim (\alpha_{mc}-\alpha)^{-\zeta_2^m}$ as $\alpha \to \alpha_{mc}+$	1

scales related to the boundary layers of the density profile. We find that, near the phase boundary between the L and LM phases, the coth boundary layer in the L phase exhibits an algebraic decay to satisfy the right boundary condition. The coth boundary layer approaches the bulk density, on the left, exponentially. The length scale associated with this exponential approach diverges near this phase boundary. The same algebraic decay is seen in the boundary layer near $x=1$ in the LM phase. This analysis makes it clear how the coth type boundary layer in the L phase transforms into an algebraically decaying boundary layer, suitable for the LM phase, as the phase boundary between the L and LM phase is approached. By particle-hole symmetry, the behavior is the same near the phase boundary between the H and HM phases. Apart from this, the transition from the LM or HM phases to the LMH phase is associated with a divergence of a length scale with an exponent -1. Similar divergences are seen in the length scales as one approaches the phase boundaries of the LM or HM phases from the M phase. In addition to this, we also show that the low- and high-density phases exist in two different surface phases with distinctly different surface layers in the density profile. Across this surface transition, a length scale ξ, associated with the location of the boundary layer, diverges logarithmically. The surface transition line and the phase boundary between the low-density and the shock phase meet at a critical point. These two lines are symmetric about the critical point and hence the shapes of these lines near the critical point are described by the same critical exponents. Although the analysis is based on a particular model, our discussion is sufficiently general and it can be implemented in more complex problems and other nonequilibrium situations.

APPENDIX A: PHASE-PLANE ANALYSIS FOR EQUATION (51)

In terms of p and f, second order equation (51) can be decomposed into two coupled first order equations

$$\frac{df}{dx^*} = p, \tag{A1}$$

$$\frac{dp}{dx^*} = f(2\Omega - p). \tag{A2}$$

$f=p=0$ is a fixed point for these equations. Linearization around this fixed point leads to the following matrix equation:

$$\frac{d}{dx^*}\begin{pmatrix}\delta f\\ \delta p\end{pmatrix} = \begin{pmatrix}0 & 1\\ 2\Omega & 0\end{pmatrix}\begin{pmatrix}\delta f\\ \delta p\end{pmatrix}, \tag{A3}$$

which can be solved through standard diagonalization scheme. The eigenvectors corresponding to the eigenvalues $(2\Omega)^{1/2}$ and $-(2\Omega)^{1/2}$ are $\binom{1}{(2\Omega)^{1/2}}$ and $\binom{1}{-(2\Omega)^{1/2}}$, respectively. The contour plots in f-p plane for different boundary conditions are presented in Fig. 10. The contour marked with the horizontal arrow satisfies the boundary conditions that are fulfilled by the boundary layer at $x=1$ in the *LM* phase. The other boundary layers joining the linear and the constant parts of the outer solutions in *LM* and *HM* phases are similarly represented by other contours in Fig. 10.

APPENDIX B: A LIST OF EXPONENTS

In Table I, ξ and x_0 are the length scales associated with the description of the virtual origin. 0 (ln) at the top of the right-most column implies a ln divergence in the notation of power law. $\chi_-^S=1/2$ in general and $\chi_-^S=1$ for $K=1$. $\{\alpha_{lc}=1/2-\Omega, \gamma<1/2\}$ is the phase boundary between the *L* and the *LM* phase. $\{\alpha>1/2, \gamma_{hc}=1/2+\Omega\}$ describes the phase boundary between the *H* and the *HM* phase. The phase boundary between the *M* phase and the *LM* phase is $\{\alpha_{mc}=1/2, \gamma<1/2\}$.

[1] G. M. Schütz, in *Phase Transitions and Critical Phenomena*, edited by C. Domb and J. Lebowitz (Academic, London, 2000), Vol. 19.

[2] T. Liggett, *Interacting Particle Systems: Contact, Voter and Exclusion Processes* (Springer-Verlag, Berlin, 1999).

[3] Sutapa Mukherji and Somendra M. Bhattacharjee, J. Phys. A **38**, L285 (2005).

[4] M. R. Evans, D. P. Foster, C. Godreche, and D. Mukamel, Phys. Rev. Lett. **74**, 208 (1995).

[5] B. Derrida *et al.*, J. Phys. A **26**, 1493 (1993); G. Schütz and E. Domany, J. Stat. Phys. **72**, 277 (1993).

[6] G. Tripathy and M. Barma, Phys. Rev. Lett. **78**, 3039 (1997); Phys. Rev. E **58**, 1911 (1998).

[7] M. R. Evans *et al.*, J. Stat. Phys. **80**, 69 (1995).

[8] J. Krug, Phys. Rev. Lett. **67**, 1882 (1991); J. S. Hager, J. Krug, V. Popkov, and G. M. Schutz, Phys. Rev. E **63**, 056110 (2001).

[9] A. Parmeggiani, T. Franosch, and E. Frey, Phys. Rev. Lett. **90**, 086601 (2003); Phys. Rev. E **70**, 046101 (2004); M. R. Evans, R. Juhasz, and L. Santen, *ibid.* **68**, 026117 (2003).

[10] S. Klumpp and R. Lipowsky, Europhys. Lett. **66**, 90 (2004); J. Stat. Phys. **113**, 233 (2003).

[11] There are differences between the results of mean field and exact solutions for the conserved case. The reasons for the differences are yet to be understood.

[12] Julian D. Cole, *Perturbation Methods in Applied Mathematics* (Blaisdell, Massachusetts, 1968).